Supporting Information

Self-Standing Non-Noble Metal (Ni-Fe) Oxide Nanotube Array Anode Catalysts with Synergistic Reactivity for High-Performance Water Oxidation

Zhenlu Zhao,[ab] Haoxi Wu,[ab] Haili He,[ab] Xiaolong Xu,[a] and Yongdong Jin*[a]

[a] State Key Laboratory of Electroanalytical Chemistry, Changchun Institute of Applied Chemistry, Chinese Academy of Sciences, Changchun, 130022, China.

[b] University of Chinese Academy of Sciences, Beijing, 100049, China.

* Corresponding author. E-mail: ydjin@ciac.ac.cn

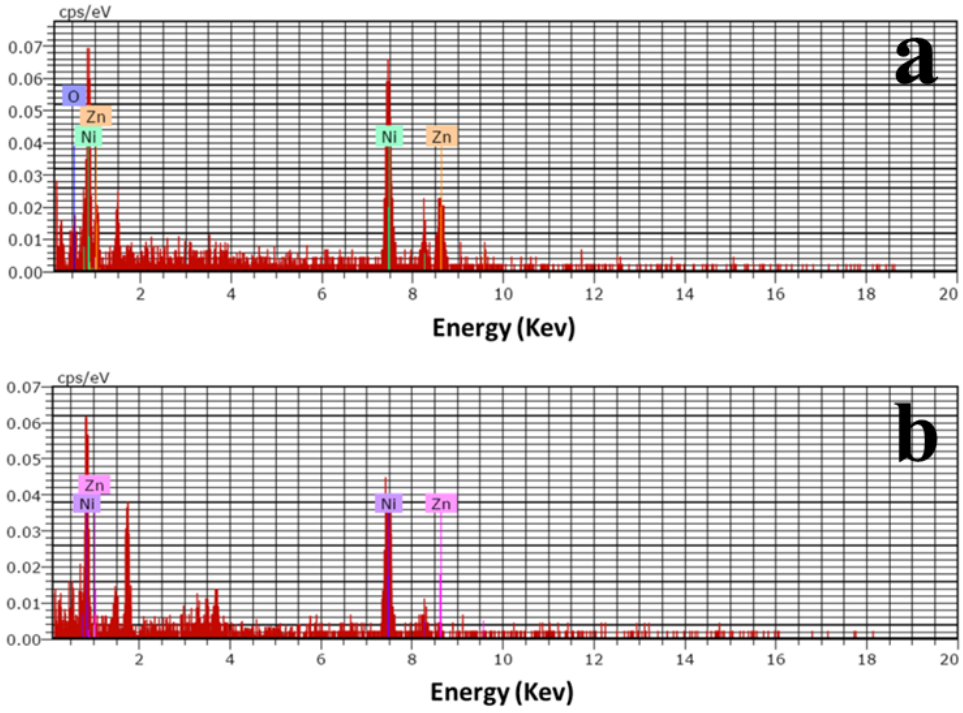

Fig. S1 EDS elemental analysis of Ni-coated ZnO NRAs (a) and ZnO-etched NNTAs (b).

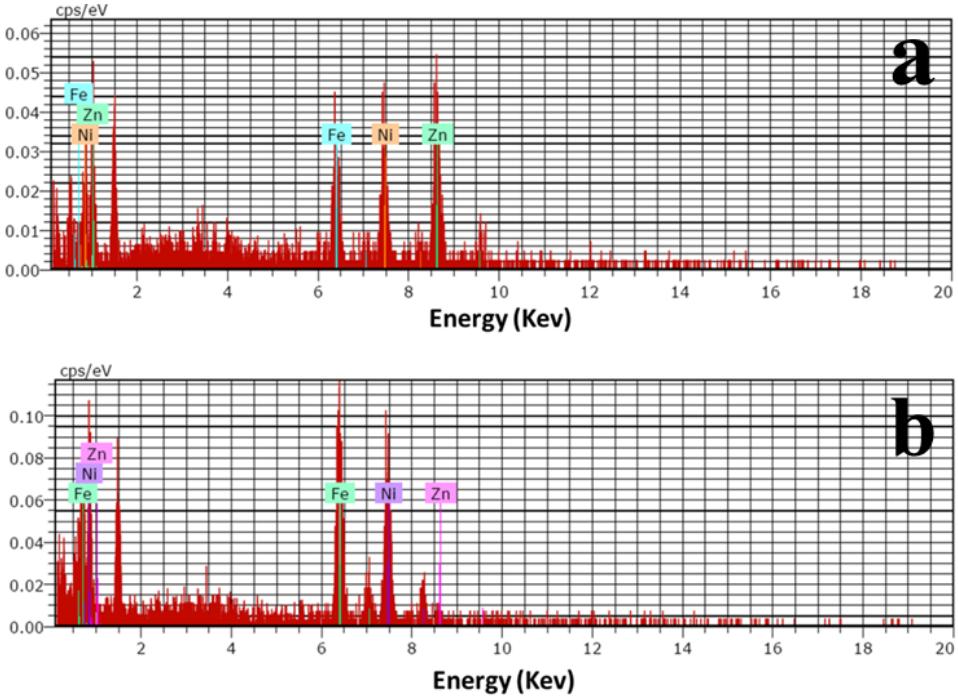

Fig. S2 EDS elemental analysis of ZNFNRAs (a) and NFNTAs (b).

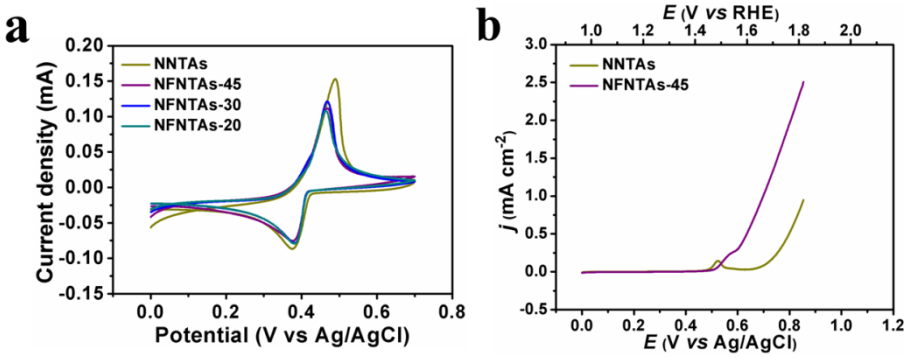

Fig. S3 (a) Cyclic voltammograms of the NNTAs, NFNTAs-45, NFNTAs-30, and NFNTAs-20 electrodes for the Ag underpotential deposition at a scan rate of 25 mV/s. (b) iR-corrected polarization curves for OER on the NNTAs and NFNTAs-45 electrodes, respectively. The current density was normalized to the electrochemically active surface area (ECSA) of the electrode which

was obtained by Ag underpotential deposition experiment. As shown in Fig. S3a, the surface areas of the NNTAs is 1.3 times larger than that of the NFNTAs-45 and the surface areas of the NFNTAs-45, NFNTAs-30, and NFNTAs-20 are almost the same.

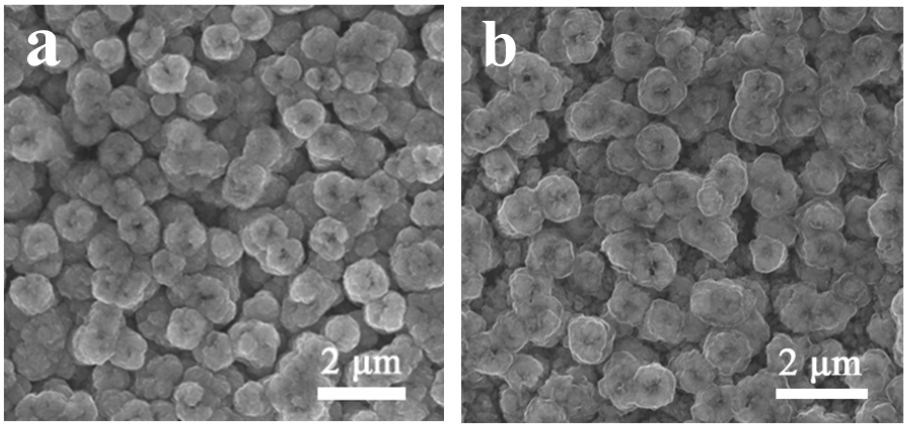

Fig. S4 Typical SEM images of the as-prepared NFNTAs-20 (a) and NFNTAs-30 (b).

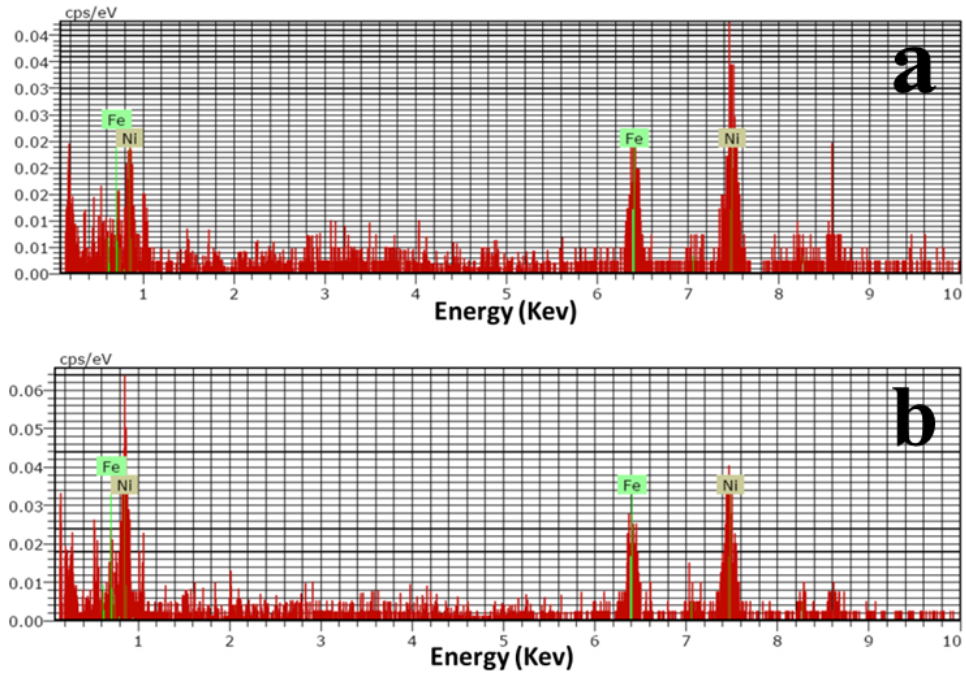

Fig. S5 EDS elemental analysis of NFNTAs-20 (a) and NFNTAs-30 (b).

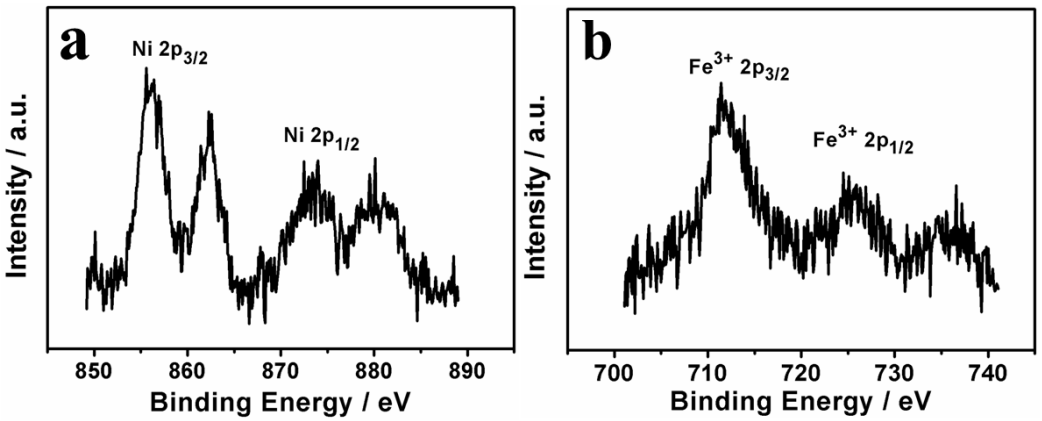

Fig. S6 (a) Ni 2p and (b) Fe 2p XPS of the NFNTAs-20.

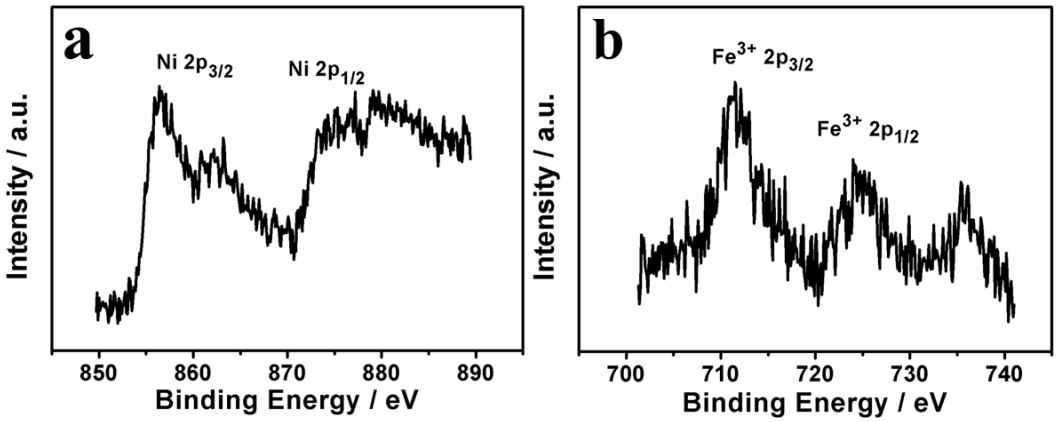

Fig. S7 (a) Ni 2p and (b) Fe 2p XPS of the NFNTAs-30.

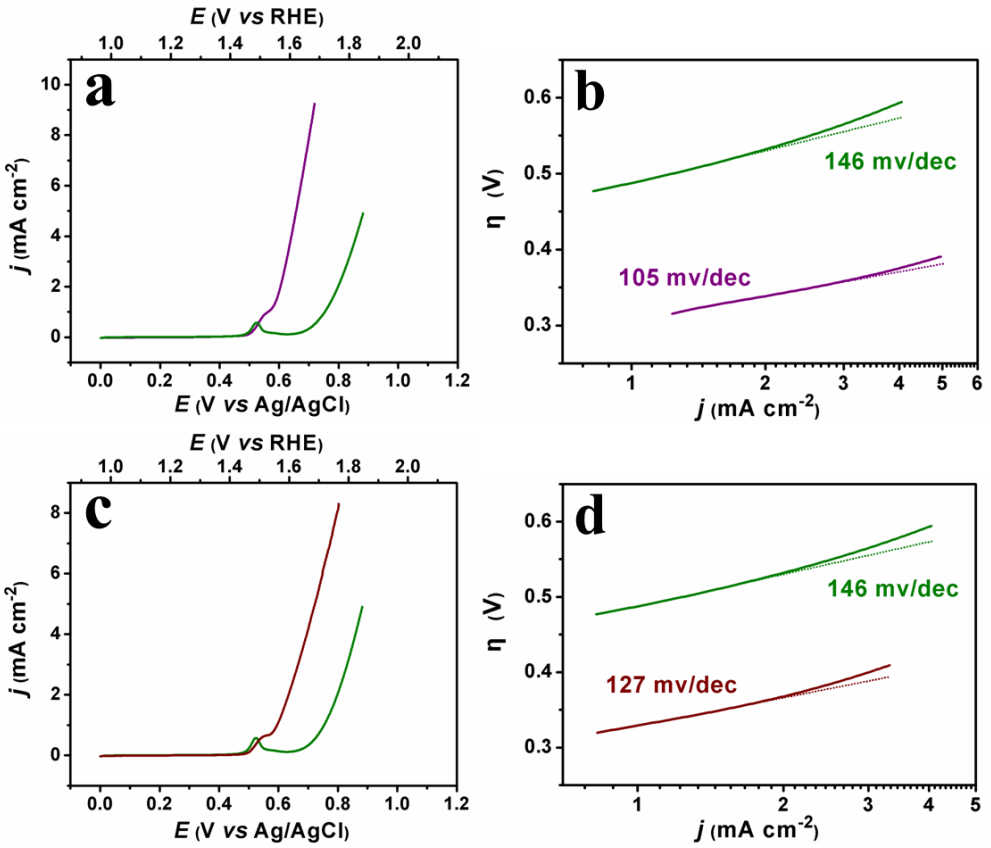

Fig. S8 (a) iR-corrected polarization curves for OER on the NFNTAs-20 (pure) and NNTAs (olive) electrodes, respectively. (b) Tafel plot overpotential versus log(j) derived from (a). (c) iR-corrected polarization curves for OER on the NFNTAs-30 (wine) and NNTAs (olive) electrodes, respectively. (d) Tafel plot overpotential versus log(j) derived from (c). All the measurements were performed in 0.1 M KOH (pH 13) at a sweep rate of 5 mV s^{-1}.

References	Materials	E [a] (V)	η [b] (V)	E [c] (V)	η [d] (V)
1	$NiCo_2S_4$@graphene	0.62	0.35	0.69	0.42
2	Meso-Co_3O_4-35	--	--	0.72	0.45
	Meso-Co_3O_4-100	0.62	0.35	0.76	0.49
3	NG-$CoSe_2$ composite	0.56	0.29	--	--
4	Ni–NG	0.59	0.32	--	--
5	MnO_x/Au-Si_3N_4	0.59	0.32	0.78	0.51
6	3D NF/PC/AN electrode	0.56	0.29	0.67	0.40
7	IrO_2 nanoparticles	0.44	0.17	0.68	0.41
This study	NFNTAs-20 electrode	0.55	0.28	0.65	0.38

[a] Onset potential (vs. Ag/AgCl); [b] Overpotential at onset potential; [c] Potential at 5 mA cm^{-1} (vs. Ag/AgCl); [d] Overpotential at 5 mA cm^{-1}. Note: the potential of the reference 7 is converted to the potential versus Ag/AgCl electrode.

Table S1 OER catalytic activity of the NFNTAs-20 electrode compared to previous transition-metal oxide materials with high catalytic activity in basic solution.

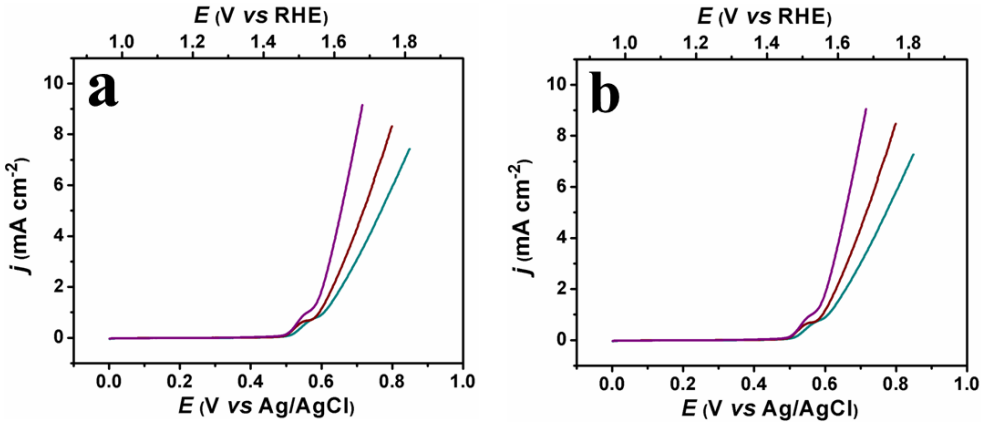

Fig. S9 (a,b) iR-corrected polarization curves for OER on the NFNTAs-45 (dark cyan), NFNTAs-30 (wine), and NFNTAs-20 (purple) electrodes, respectively. All the measurements were performed in 0.1 M KOH (pH 13) at a sweep rate of 5 mV s^{-1}.

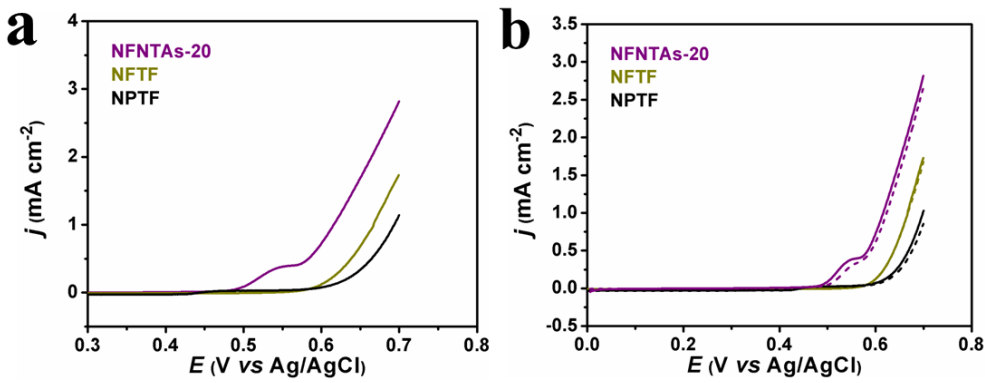

Fig. S10 (a) IR-corrected polarization curves for OER on the NFNTAs-20 electrode, NFTF electrode and NPTF electrode, respectively. (b) IR-corrected OER polarization curves for the NFTF and NPTF electrodes before (solid line) and after (dashed line) 500 cycles of accelerated stability test. All the measurements were performed in 0.1 M KOH (pH 13) at a sweep rate of 5 mV s^{-1}. The NFTF was electrodeposited on ITO for 40 min in a mixed solution of $NiSO_4$ (0.02 M), NH_4Cl (0.04 M) and $FeSO_4$ (0.005 M) (current density: 0.35 mA cm^{-2}, electrode area: 0.283 cm^{-2}). The NPTF electrode was obtained by drop-coating the sample (6 mg ml^{-1}, water:5 wt% Nafion solution=10:1) to completely cover the ITO surface (electrode area: 0.283 cm^{-2}). The current density was normalized to the electrochemically active surface area (ECSA) of the electrode which was obtained by Ag underpotential deposition experiment.

Reference

1. Q. Liu, J. Jin and J. Zhang, *ACS Appl. Mater. Interfaces*, 2013, **5**, 5002-5008.
2. H. Tüysüz, Y. Hwang, S. Khan, A. Asiri and P. Yang, *Nano Res.*, 2013, **6**, 47-54.
3. M.-R. Gao, X. Cao, Q. Gao, Y.-F. Xu, Y.-R. Zheng, J. Jiang and S.-H. Yu, *ACS Nano*, 2014, **8**, 3970–3978.
4. S. Chen, J. Duan, J. Ran, M. Jaroniec and S. Z. Qiao, *Energy Environ. Sci.*, 2013, **6**, 3693-3699.
5. Y. Gorlin, B. Lassalle-Kaiser, J. D. Benck, S. Gul, S. M. Webb, V. K. Yachandra, J. Yano and T. F. Jaramillo, *J. Am. Chem. Soc.*, 2013, **135**, 8525–8534.
6. J. Wang, H.-X. Zhong, Y.-L. Qin and X.-B. Zhang, *Angew. Chem. Int. Ed.*, 2013, **52**, 5248-5253.
7. Y. Lee, J. Suntivich, K. J. May, E. E. Perry and Y. Shao-Horn, *J. Phys. Chem.Lett.*, 2012, **3**, 399-404.